

# Measuring parameters of AGN central engines with very high energy $\gamma$ -ray flares

A. Neronov<sup>1,2</sup>, D. Semikoz<sup>3,4</sup>, S. Sibiryakov<sup>5,4</sup>

<sup>1</sup>INTEGRAL Science Data Center, Chemin d’Écogia 16, 1290 Versoix, Switzerland

<sup>2</sup>Geneva Observatory, 51 ch. des Maillettes, CH-1290 Sauverny, Switzerland

<sup>3</sup>APC, 10, rue Alice Domon et Leonie Duquet, 75205 Paris, France

<sup>4</sup>Institute for Nuclear Research of the Russian Academy of Sciences, 60th October Anniversary prospect 7a, Moscow 117312, Russia

<sup>5</sup>Theory Group, Physics Department, CERN, CH-1211 Geneva 23, Switzerland

Received <date>; in original form <date>

## ABSTRACT

We discuss a “compact source” model of very high energy (VHE) emission from blazars in which the variability time is determined by the blazar central engine. In this model electron or proton acceleration close to the supermassive black hole is followed by the development of electromagnetic cascade in a radiatively inefficient accretion flow. Assuming such a model for the TeV blazar PKS 2155-304, we show that the variability properties of the TeV  $\gamma$ -ray signal observed during a bright flare from this source, such as the minimal variability time scale and the recurrence period of the sub-flares, constrain the mass and the angular momentum of the supermassive black hole.

**Key words:** gamma-rays: theory, galaxies: nuclei, radiation mechanisms: non-thermal, black hole physics, BL Lacertae objects: individual: PKS 2155-304

## 1 INTRODUCTION

Recent observation of fast variability of TeV  $\gamma$ -ray emission from several TeV blazars (Aharonian et al. 2007; Albert et al. 2007) challenges the conventional model in which the TeV  $\gamma$ -rays are supposed to be produced at large distances from the blazar central engine, the supermassive black hole. Within this conventional model the  $\gamma$ -ray emitting blobs are assumed to travel to the parsec-scale distances along the AGN jet before emitting in the TeV energy band; it is believed that otherwise the  $\gamma$ -ray emission would be strongly absorbed in the accretion flow (see e.g. Ghisellini & Madau (1996)). Since the radiative cooling time of the TeV emitting electrons is typically shorter than the time of propagation from the central engine to the TeV emission region, it is usually assumed that the TeV emitting particles are produced via shock acceleration locally in the emission region, rather than in the AGN central engine.

At the same time, the observed short variability time scales  $t_{\text{var}} \sim$  a few minutes indicate that the TeV emission comes from very compact regions having the size in the co-moving frame  $\Delta x' \lesssim \delta(1+z)^{-1}ct_{\text{var}}$ , where  $\delta$  is the bulk Doppler factor and  $z$  is the source redshift. This implies that in the static frame the longitudinal size of the TeV emitting region is

$$\Delta x = \frac{\Delta x'}{\Gamma} \lesssim (1+z)^{-1}ct_{\text{var}} \simeq 6 \times 10^{12}(1+z)^{-1} \left[ \frac{t_{\text{var}}}{200 \text{ s}} \right] \text{ cm}. \quad (1)$$

where we assume that the bulk Lorentz factor  $\Gamma \sim \delta$ . This is comparable to the minimal possible scale set up by the gravitational radius of the central supermassive black hole

$$R_g = GM_{\text{BH}}/c^2 \simeq 1.5 \times 10^{12} [M_{\text{BH}}/10^7 M_{\odot}] \text{ cm}. \quad (2)$$

Even if one assumes that the TeV emitting plasma blobs are produced close to the black hole, which would explain their initially small size, it is not clear how the blobs propagating downstream the relativistic jet can retain this size up to large distances, unless they have unreasonably large bulk Lorentz factors. This problem has recently led to a suggestion (Begelman et al. 2008) that the TeV flares may be not triggered by the black hole but rather are results of enhanced emission intrinsic to the jet.

However even in that case, to explain the observed rapid variability, the TeV  $\gamma$ -ray emitting blobs have to travel with quite large bulk Lorentz factors,  $\Gamma \gg 1$ . Such Lorentz factors are in contradiction with the radio observations of the motion of hot spots in the parsec-scale jets. Moderate apparent speeds of the blobs of the parsec-scale jets, revealed by radio observations, combined with an estimate of the number of parent objects of TeV blazars, would give much smaller values of the bulk Lorentz factors,  $\Gamma \sim 1$  (Henri & Saugé 2006). For example, to explain the fast variability of the July 2006 TeV flare of PKS 2155-304 (Aharonian et al. 2007) the bulk Lorentz factor required by the mechanism of TeV emission in the parsec-scale jet should be  $\Gamma > 50$  (Aharonian et al. 2007; Begelman et al. 2008). At the same time, the direct

observations of the apparent velocity of hot spots in PKS 2155-304 jet at the projected distance ( $1 \div 2$ ) parsecs give the value  $v_{\text{app}} = (0.9 \pm 0.3)c$  (Piner et al. 2008). Assuming that the viewing angle is not too small,  $\theta \gtrsim 1^\circ$ , this yields  $\Gamma \lesssim 10$  at the distance of a few tens of parsecs from the central engine.

Both the problems of the fast variability and of the small observed Lorentz factors at parsec distances could be naturally resolved if the site of the VHE  $\gamma$ -ray production is located closer to the AGN central engine, at significantly sub-parsec distances. If the VHE emitting region is moving relativistically toward the observer with a bulk Lorenz factor  $\Gamma$ , the variability time scale limits the distance  $R$  of the  $\gamma$ -ray production site from the central engine (see e.g. Celotti et al. (1998)),

$$R \sim \Delta x \Gamma^2 \leq 1.5 \times 10^{16} (1+z)^{-1} \left[ \frac{t_{\text{var}}}{200 \text{ s}} \right] \left[ \frac{\Gamma}{50} \right]^2 \text{ cm.} \quad (3)$$

An immediate difficulty is, however, that at such distances the accretion flow onto the black hole can be opaque to the  $\gamma$ -rays (see e.g. Blandford & Levinson (1995)).

The problem of opacity of the compact source does not arise in the case of low-luminosity AGNs that accrete at significantly sub-Eddington rates (Celotti et al. 1998). In these sources the accretion flow is described within the framework of the radiatively inefficient accretion flow (RIAF) models (Rees et al. 1982; Narayan & Yi 1994, 1995; Narayan 2002) in which most of the gravitational energy extracted from the accreted matter is converted into internal energy, rather than into radiation. The possibility of escape of the VHE  $\gamma$ -rays from the vicinity of the AGN central engine is best illustrated by the nearby low-luminosity radio galaxy M87, which was recently found to be a source of the variable TeV  $\gamma$ -ray emission (Aharonian et al. 2003, 2006; Albert et al. 2008), most probably coming from a compact source (Neronov & Aharonian 2007; Rieger & Aharonian 2008b).

In the compact source model the VHE  $\gamma$ -ray emission is triggered by high-energy particles accelerated close to the black hole via one of the possible mechanisms (see e.g. Lovelace (1976); Lesch & Pohl (1992); Kardashev (1995); Bednarek & Protheroe (1999); Neronov et al. (2002); Neronov & Semikoz (2002); Neronov et al. (2005); Rieger & Aharonian (2008a); Neronov et al. (2008)). In this case the spectral and timing characteristics of the VHE emission are directly linked to the physics of the processes taking place close to the supermassive black hole, which naturally explains the variability of the signal on the shortest possible time scale.

Within the AGN unification scheme, the TeV blazars (high-energy peaked BL Lacs) are assumed to be the beamed versions of the low-luminosity radio galaxies similar to M87 (Browne 1983; Giroletti et al. 2004, 2006). Since the only difference between the TeV blazars and the low-luminosity radio galaxies is their orientation with respect to the line of sight, the compact source model can be applicable also in the case of TeV blazars.

In what follows we adopt this point of view and develop a compact source model of high-energy activity of TeV blazars. We demonstrate that within such compact source model the characteristics of the fast-variable VHE emission can be used to constrain the parameters of the AGN cen-

tral engine, in particular, the density and luminosity of the accretion flow, the black hole mass and spin. We illustrate this possibility on the particular example of the bright PKS 2155-304 flare detected by the HESS telescope in July 2006 (Aharonian et al. 2007). This flare consists of a number of well-pronounced sub-flares which exhibit quasi-periodic recurrence. We show that the rise time and the recurrence period of the sub-flares can be directly related to the light-crossing time and to the period of rotation over the last stable orbit around a  $M_{\text{BH}} \sim 10^7 M_{\odot}$  black hole<sup>1</sup>.

The paper is organized as follows. In Sec. 2 we discuss the qualitative features of the model, including particle acceleration and propagation through the RIAF environment. The possibility of a new interpretation of the observational data within such a model is demonstrated in Sec. 3 where we find the constraints on the black hole mass and angular momentum imposed by the timing analysis of the bright TeV flare of PKS 2155-304. We summarize our results in Sec. 4.

## 2 COMPACT SOURCE MODEL OF THE TEV BLAZARS

In the compact source model the VHE  $\gamma$ -ray emission region is assumed to be situated in the vicinity of the AGN central engine, rather than at parsec-scale distances. This fact implies two main differences of this model from a generic "relativistically moving blob" model of VHE emission from blazars. First, the high-energy particles responsible for the VHE emission can be injected into the  $\gamma$ -ray emission region by the AGN central engine, rather than only by a process (shock acceleration) intrinsic to the blob. Second, the characteristics of the  $\gamma$ -ray emission are determined not only by the intrinsic properties of the blob, but also by the effects of propagation of the high-energy particles through the matter and radiation environment created by the accretion flow. However, as we discuss below, the compact source model to some extent includes the blob model: the electromagnetic cascade, which develops as a result of the propagation of high-energy particles through the accretion flow environment, leads to the formation of a relativistically moving blob of secondary cascade particles. In the following sub-sections we consider general features of particle acceleration and propagation in the compact source model of TeV blazars.

### 2.1 Particle acceleration and "direct" $\gamma$ -ray emission from the acceleration region

A number of mechanisms of particle acceleration in the vicinity of the central black hole have been proposed in the literature (see e.g. Lovelace (1976); Lesch & Pohl (1992); Kardashev (1995); Bednarek & Protheroe (1999); Neronov et al. (2002); Neronov & Semikoz (2002); Neronov et al. (2005); Rieger & Aharonian (2008a); Neronov et al. (2008)). In this sub-section we summarize some common features of the acceleration models which

<sup>1</sup> This mass estimate is different from the value  $\sim 10^9 M_{\odot}$  quoted by Aharonian et al. (2007). We will comment on this discrepancy in Sec. 3.3.

are related to the fact that the acceleration proceeds in a compact region of the size comparable to the black hole horizon and are independent of the details of the acceleration mechanism.

A conventional dimensional estimate of maximal possible energies of particles of charge  $e$  accelerated in a region of the size  $R \sim R_g$  with the magnetic field  $B$  is

$$E_{\max} = \kappa e B R_g \simeq 10^{19} \kappa \left[ \frac{B}{10^4 \text{ G}} \right] \left[ \frac{M_{\text{BH}}}{10^7 M_{\odot}} \right] \text{ eV}, \quad (4)$$

where  $\kappa \leq 1$  is the efficiency of a particular acceleration mechanism. This maximal energy is, however, not always achieved because of the strong energy losses experienced by the accelerated particles. The "minimal" energy loss channel is the loss on the curvature radiation (Levinson 2000; Aharonian & Neronov 2005; Neronov et al. 2008), which limits the particle energies to

$$\frac{E_{\text{cur}}}{mc^2} \leq \left[ \frac{3R_g^2 \kappa B}{2e} \right]^{1/4} \simeq 3 \times 10^9 \kappa^{1/4} \left[ \frac{M_{\text{BH}}}{10^7 M_{\odot}} \right]^{1/2} \left[ \frac{B}{10^4 \text{ G}} \right]^{1/4} \quad (5)$$

where  $m$  is the particle mass. Here we normalize the magnetic field to the value  $10^4$  G typical for the central engine of an AGN with a  $10^7 M_{\odot}$  black hole. Additional energy losses, caused by the interactions of the accelerated particles with the matter and radiation backgrounds produced by the accretion flow (see Sec. 2.2 below), lead to further reduction of the maximal attainable energy. If the magnetic field in the acceleration region is not ordered, the energies of the accelerated particles are reduced because of the strong synchrotron energy loss.

Radiative energy losses which accompany particle acceleration (curvature, synchrotron, inverse Compton) result in the  $\gamma$ -ray emission directly from the acceleration region. If the resulting  $\gamma$ -rays are not completely absorbed during their propagation through the photon background created by the accretion flow, this "direct"  $\gamma$ -ray emission can, in principle, provide an observable signature of the compact source model. We will return to this point in Sec. 2.4.

Since the maximal energies of particles are determined by the balance of the acceleration and energy loss rates, all the work done by the electric field is dissipated via the available energy loss channels. For each charged particle the energy loss rate is about the acceleration rate,  $dE/dt \sim e\kappa B c$ , where we assume that the accelerating electric field strength is  $\sim \kappa B$ . The maximal possible density of particles in the acceleration region,  $n_q \sim \kappa B/eR$ , is determined by the condition that a charge redistribution cannot screen the electric field. One estimates the total power extracted from the acceleration region by multiplying the energy loss rate of each particle on the maximal possible particle density and on the volume of the acceleration region,  $V \sim R_g^3$ , this yields

$$\begin{aligned} P_{\text{tot}} &\simeq n_q R_g^3 (dE/dt) \\ &\simeq 5 \times 10^{42} \kappa^2 \left[ \frac{M_{\text{BH}}}{10^7 M_{\odot}} \right]^2 \left[ \frac{B}{10^4 \text{ G}} \right]^2 \text{ erg/s.} \end{aligned} \quad (6)$$

Comparing this estimate to the apparent luminosity of a bright TeV flare (found under the assumption that the radiation is isotropic),  $L_{\text{iso}} \simeq 10^{46} \text{ erg/s}$ , one concludes that the energetics of such a flare is compatible with the compact source model if the TeV emission is beamed into the solid angle  $\Omega/4\pi \lesssim 10^{-3}$ . The emission from the compact

source is expected to be anisotropic, with the direction of the beam of high-energy particles and/or photons set up by the direction of the magnetic field.

A fraction of the work done by the accelerating electric field is carried away by the flux of accelerated particles (a relativistic wind). In the case of electrons, this fraction is usually negligible. In the case of protons or heavy nuclei the power of the relativistic particle wind,  $P_p$ , can be estimated as

$$\begin{aligned} P_p &\sim n_q R_g^2 c \cdot \min\{E_{\text{cur}}, E_{\max}\} \\ &\simeq \begin{cases} 10^{42} \kappa^{5/4} \left[ \frac{M_{\text{BH}}}{10^7 M_{\odot}} \right]^{3/2} \left[ \frac{B}{10^4 \text{ G}} \right]^{5/4} \frac{\text{erg}}{\text{s}}, & E_{\text{cur}} < E_{\max} \\ 5 \times 10^{42} \kappa^2 \left[ \frac{M_{\text{BH}}}{10^7 M_{\odot}} \right]^2 \left[ \frac{B}{10^4 \text{ G}} \right]^2 \frac{\text{erg}}{\text{s}}, & E_{\text{cur}} > E_{\max} \end{cases} \end{aligned} \quad (7)$$

This order-of-magnitude estimate does not take into account a possible special geometry of the accelerating field. If, for instance, particles are accelerated in parallel magnetic and electric fields in the polar cap regions of black hole magnetospheres, the curvature radii of particle trajectories can be somewhat larger than  $R_g$  and, respectively, the maximal attainable energies and the power of the particle beam can be higher (Neronov et al. 2008).

The high-energy particles and radiation emitted from the acceleration region are injected into the accretion flow. The form of the  $\gamma$ -ray signal produced by the interaction of the accelerated particles with the radiation coming from the accretion flow depends sensitively on the geometry of the central engine. The precise determination of this signal should involve detailed numerical modeling which is beyond the scope of the present paper. Below we limit ourselves to order-of-magnitude estimates which highlight the qualitative features of the problem.

## 2.2 Radiatively inefficient accretion flow

In this subsection we summarize the general properties of the radiation produced by the accretion flow. As it is mentioned in the Introduction, the TeV blazars belong to the class of low-luminosity radio galaxies in which the accretion is conventionally described in the framework of RIAF models (see e.g. Narayan (2002) and references therein) relevant for sources in which the accretion rate  $\dot{M}$  is small in the Eddington units,

$$\dot{M} \ll \dot{M}_{\text{Edd}} \equiv \frac{L_{\text{Edd}}}{0.1 c^2} \simeq 0.2 \left[ \frac{M_{\text{BH}}}{10^7 M_{\odot}} \right] M_{\odot}/\text{yr}, \quad (8)$$

where  $\dot{M}_{\text{Edd}}$  is the Eddington accretion rate.

The low radiative efficiency of the accretion flow is attributed to the low matter density which leads to inefficient cooling of electrons and ions in the accretion flow. As a result, a large fraction of the released gravitational energy, instead of being dissipated in the form of radiation, is stored in the internal energy of matter. This energy either disappears under the horizon or is ejected in an outflow.

Large internal energy of matter does not allow formation of a geometrically thin, optically thick accretion disk. Instead, the accreting matter forms around the BH a hot optically thin gaseous torus (Rees et al. 1982). In RIAF models the accretion torus typically consists of two-temperature plasma with both electrons and ions being mildly relativistic. The radiation of the plasma is entirely produced by

electrons via three main mechanisms: synchrotron radiation, comptonization of the latter, and bremsstrahlung.

The synchrotron radiation contributes to the far infrared part of the spectrum. The characteristic synchrotron emission energy is

$$\epsilon_{\text{synch}} = \frac{\hbar e B}{m_e c} \langle \gamma_e^2 \rangle \simeq 5 \times 10^{-3} \left[ \frac{B}{10^4 \text{ G}} \right] \left[ \frac{T_e}{1 \text{ MeV}} \right]^2 \text{ eV} , \quad (9)$$

where  $B$  is the magnetic field in the inner part of the accretion torus,  $m_e$  is the electron mass,  $\langle \gamma_e^2 \rangle$  is the mean-square  $\gamma$ -factor of electrons,  $T_e$  is the electron temperature, and we have used that for mildly relativistic electrons

$$\langle \gamma_e^2 \rangle \sim 10 \left( \frac{T_e}{m_e c^2} \right)^2 . \quad (10)$$

One of the parameters of the RIAF models is the ratio  $\beta$  of the gas pressure  $p_{\text{gas}} = n m_p v_{\text{th}}^2 / 3$  to the magnetic pressure  $p_{\text{magn}} = B^2 / 4\pi$ . Here  $n$  is the gas density,  $m_p$  is the proton mass and  $v_{\text{th}}$  is the thermal velocity of protons which can be estimated as the Keplerian velocity at the corresponding distance,  $v_{\text{th}}(R) \approx (R_g/R)^{1/2}$ . With the use of parameter  $\beta$ , the magnetic field is estimated as

$$\begin{aligned} B(R) &= \left[ \frac{4\pi}{3} \beta^{-1} n(R) m_p v_{\text{th}}^2(R) \right]^{1/2} \\ &\simeq 10^4 \beta^{-1/2} \left[ \frac{R_g}{R} \right]^{1/2} \left[ \frac{n(R)}{10^{10} \text{ cm}^{-3}} \right]^{1/2} \text{ G} . \end{aligned} \quad (11)$$

Note that we normalize the matter density in the black hole vicinity to the value  $10^{10} \text{ cm}^{-3}$ , typical for the case of a  $10^7 M_\odot$  black hole in the RIAF models, cf. Narayan & Yi (1995).

If the matter density changes with the distance as  $n(R) \sim R^{-\gamma}$  (in the RIAF models  $1/2 \leq \gamma \leq 3/2$  (Lu et al. 2004)) the magnetic field decreases as  $B \sim R^{-(\gamma+1)/2}$ , so that the synchrotron cooling time

$$t_{\text{synch}} = \frac{6\pi m_e c^2}{\sigma_T B^2 \gamma_e} \simeq 1.3 \left[ \frac{B}{10^4 \text{ G}} \right]^{-2} \left[ \frac{T_e}{1 \text{ MeV}} \right]^{-1} \text{ s} \quad (12)$$

increases with the distance as  $t_{\text{synch}} \sim R^{(\gamma+1)}$ . Here  $\sigma_T = 0.665 \times 10^{-24} \text{ cm}^2$  is the Thomson cross-section. The synchrotron cooling is efficient only close to the BH horizon. Indeed, the synchrotron cooling time grows with  $R$  faster than the dynamical time scale given by the free-fall time,

$$t_{\text{ff}} \simeq \sqrt{R^3 / GM_{\text{BH}}} \quad (13)$$

Thus, the bulk of the synchrotron emission is produced in the vicinity of the horizon. Numerical simulations (Narayan 2002) confirm this qualitative result.

The synchrotron emission in the RIAF models is damped due to self-absorption. The self-absorption coefficient has the form (Pacholczyk 1970)

$$\alpha_{\text{SA}}(\epsilon) = \frac{\pi \hbar e^2 m^2 c^5 n}{2\sqrt{3} T_e^3 \epsilon} I(x) , \quad (14)$$

where

$$x = \frac{2m^3 c^5 \epsilon}{3\hbar e B T_e^2} \quad (15)$$

and the function  $I(x)$  is given explicitly in the appendix A. Equating  $\alpha_{\text{SA}}^{-1}$  to the size of the synchrotron emission region, which we take to be of order of the gravitational radius, one

finds the photon energy at which the synchrotron emission becomes optically thin

$$\epsilon_{\text{SA}} \simeq 37 \epsilon_{\text{synch}} . \quad (16)$$

As discussed in the appendix A, the numerical coefficient in this formula mildly depends on the parameters of the accretion flow. We omit this dependence in what follows.

Since  $\epsilon_{\text{SA}} > \epsilon_{\text{synch}}$ , the maximum of the synchrotron power is emitted at the energy  $\epsilon_{\text{SA}}$ . To estimate the synchrotron luminosity we approximate the spectrum by thermal radiation up to  $\epsilon_{\text{SA}}$ . This yields

$$L_{\text{synch}} = 4\pi R_{\text{synch}}^2 \frac{2T_e}{c^2} \int_0^{\epsilon_{\text{SA}}} \frac{\epsilon^2 d\epsilon}{(2\pi\hbar)^3} , \quad (17)$$

where  $R_{\text{synch}}$  is the size of the synchrotron emission region. Substituting  $R_{\text{synch}} \approx R_g$  we obtain

$$L_{\text{synch}} \simeq 3.2 \times 10^{39} \left[ \frac{M_{\text{BH}}}{10^7 M_\odot} \right]^2 \left[ \frac{B}{10^4 \text{ G}} \right]^3 \left[ \frac{T_e}{1 \text{ MeV}} \right]^7 \text{ erg/s} . \quad (18)$$

The part of the synchrotron spectrum above  $\epsilon_{\text{SA}}$  gives small contribution to the total synchrotron power because of the exponential cutoff in the synchrotron emission function. An immediate consequence of this cutoff is that the bulk of the synchrotron photons have energies  $\epsilon \lesssim \epsilon_{\text{SA}} \simeq 0.2 \text{ eV}$ .

The synchrotron radiation is upscattered by inverse Compton (IC) process into the optical band,

$$\epsilon_{\text{IC}} \sim \epsilon_{\text{SA}} \langle \gamma_e^2 \rangle \simeq 4 \left[ \frac{B}{10^4 \text{ G}} \right] \left[ \frac{T_e}{1 \text{ MeV}} \right]^4 \text{ eV} . \quad (19)$$

To estimate the luminosity of the accretion flow in this range we note that the IC volume emissivity at distance  $R$  from the black hole is (Rybicki & Lightman 2004)

$$\frac{dL_{\text{IC}}}{dV} = \frac{4}{3} \sigma_T c n(R) \langle \gamma_e^2(R) \rangle U_{\text{synch}}(R) , \quad (20)$$

where  $\langle \gamma_e^2(R) \rangle$  is the mean-square gamma-factor of electrons at this distance, and  $U_{\text{synch}}(R) \simeq L_{\text{synch}} / (4\pi R^2 c)$  is the energy density of the synchrotron radiation. Integrating over the volume we obtain

$$L_{\text{IC}} \simeq \frac{4}{3} L_{\text{synch}} \sigma_T \int n_e(R) \langle \gamma_e^2(R) \rangle dR . \quad (21)$$

Depending on the radial profiles of the electron density and temperature, the integral in (21) is saturated either close to the black hole horizon (for the radial profiles steeper than  $n(R) \langle \gamma_e^2(R) \rangle \sim R^{-1}$ ) or in a region which is much larger than the size of the black hole. In the numerical simulations of RIAF models one finds the typical size  $R_{\text{IC}}$  of the IC emission region to be of order  $100 R_g$  (Narayan 2002). As a crude estimate let us consider the case when the integral in (21) is saturated at the upper limit. Then,

$$\begin{aligned} L_{\text{IC}} \simeq 0.4 \times 10^{39} &\left[ \frac{L_{\text{synch}}}{10^{39} \text{ erg/s}} \right] \left[ \frac{R_{\text{IC}}}{10^{14} \text{ cm}} \right] \\ &\times \left[ \frac{n(R_{\text{IC}})}{10^8 \text{ cm}^{-3}} \right] \left[ \frac{T_e(R_{\text{IC}})}{1 \text{ MeV}} \right]^2 \text{ erg/s} . \end{aligned} \quad (22)$$

Note that in the above estimate we took into account that the electron density and temperature at the distance  $R_{\text{IC}}$  are lower than near the black hole.

Finally, we consider the bremsstrahlung radiation. It contributes primarily into the X-ray/soft  $\gamma$ -ray band with

the total power typically comparable or lower than that of the synchrotron radiation. The bremsstrahlung emission power is proportional to  $n^2$ , so that the bremsstrahlung luminosity from a region of the size  $R$  is  $P_{\text{brems}} \sim n(R)^2 R^3$ . If the radial density falls down slower than  $n(R) \sim R^{-3/2}$  (as it is the case in typical RIAF models), the bulk of the bremsstrahlung flux is produced at large distances. Numerical modeling of the radiatively inefficient accretion shows that the bremsstrahlung is produced mainly at large distances from the BH,  $R_{\text{brems}} \sim 10^5 \times R_g$  (Narayan 2002).

To summarize, the properties of RIAF important for the high-energy particle propagation are as follows. Matter distribution in a typical RIAF is characterized by a rather shallow radial density profile  $n(R) \sim R^{-1/2} \div R^{-3/2}$ , so that the central matter density is rather low. At the same time, due to the large non-dissipated mechanical energy of the accreting matter the magnetic field produced by the RIAF can be strong close to the central black hole (11). The radiation environment created by a RIAF has an "onion-like" structure with the infrared synchrotron emission produced close to the black hole, infrared/optical IC emission produced in a larger region of the size  $\sim 100R_g$  and X-ray/soft  $\gamma$ -ray bremsstrahlung emission produced in a region of the size  $\sim 10^5 R_g$ .

To conclude this section let us make the following comment. The estimates presented above strongly depend on the values of the parameters of the accretion flow such as electron temperature, density and magnetic field. These characteristics vary significantly in different RIAF models. The estimates presented in this section should be considered as indicative. A more detailed analysis of the the radiative background can be done using numerical simulations in each particular RIAF model.

### 2.3 Propagation of the high-energy particles through the accretion flow background

The compact particle accelerator close to the black hole produces emission with the total power  $P_{\text{tot}}$ , Eq. (6). As discussed above, the partition of this energy between the  $\gamma$ -ray component and the accelerated matter depends on the type of accelerated particles, see Fig. 1. If the accelerated particles are electrons the power goes completely into  $\gamma$ -rays, while in the case of the proton acceleration a significant part of  $P_{\text{tot}}$  can remain in the high-energy particle beam, see Eq. (7). The primary  $\gamma$ -rays and protons propagate through and interact with the matter and radiation background created by RIAF. Interactions of high-energy particles give rise to electromagnetic cascades that redistribute the power initially contained in the highest energy particles to lower energy bands. Since the rates of interactions of electrons and  $\gamma$ -rays are significantly different from those of protons, we consider these two cases separately.

#### 2.3.1 Electrons and $\gamma$ -rays

The highest energy  $\gamma$ -rays produce pairs in interactions with the soft photon background inside the compact source. The cross-section of photon–photon pair-production depends on the center-of-mass energy of colliding photons,

$$s = E\epsilon(1 - \cos\theta)/2m_e^2, \quad (23)$$

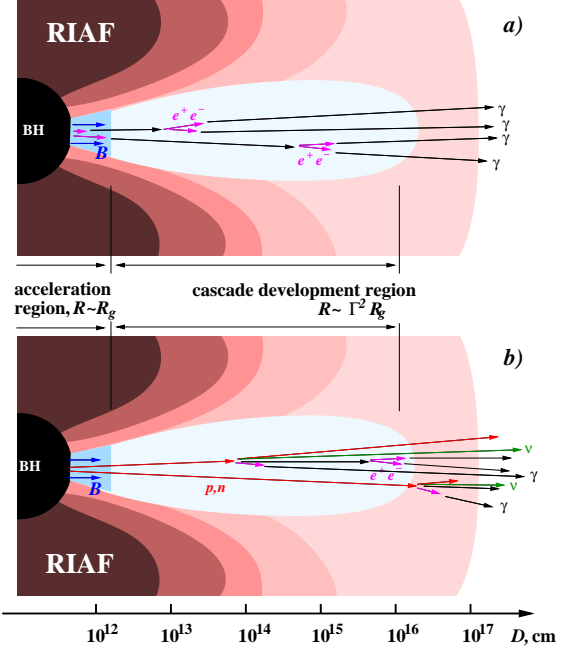


**Figure 1.** Schematic representation of the two possible scenarios for the  $\gamma$ -ray emission from the compact source. Particles (electrons in the upper panel, protons in the lower panel) are initially accelerated in a compact region of the size of about  $R_g$ , shown as a blue-shaded region. Particles which escape from the acceleration region initiate a cascade in the radiatively-inefficient accretion flow, at the distances  $R \gg R_g$ , shown as a light-blue shaded region.

where  $E$  and  $\epsilon$  are the energies of the photons, and  $\theta$  is the collision angle. Starting from the threshold at  $s = 1$  the cross-section rapidly increases achieving the maximum  $\sigma_{\gamma\gamma} \approx 1.3 \times 10^{-25} \text{ cm}^2$  at  $s \approx 4$ , and then decreases as  $s^{-1} \ln s$ . Because of relatively narrow distribution of  $\sigma_{\gamma\gamma}(s)$ ,  $\gamma$ -rays interact most efficiently with the optical/infrared background photons of energy  $\epsilon \simeq 1(E_\gamma/1 \text{ TeV})^{-1} \text{ eV}$ . This interaction leads to absorption of the  $\gamma$ -rays. In order for the VHE emission to escape from the vicinity of the black hole the optical depth of this process should be less than one. Let us consider the contributions of the various backgrounds produced by RIAF to the optical depth, case by case.

We start with the synchrotron background. This background is produced in the vicinity of the black hole,  $R_{\text{synch}} \approx R_g$ . Consequently, its interaction with the VHE emission strongly depends on the geometry of the inner part of the accretion disc and of the acceleration region. The situation is still more complicated because of the exponential dependence of the density of the synchrotron background photons on energy (Pacholczyk 1970),

$$n_{\text{synch}}(\epsilon) = n_{\text{synch}}(\epsilon_{\text{SA}}) I(x)/I(x_{\text{SA}}), \quad \epsilon > \epsilon_{\text{SA}}, \quad (24)$$

where the function  $I(x)$  is given in Eq. (A2) and  $x$  is defined in Eq. (15). The density  $n_{\text{synch}}(\epsilon_{\text{SA}})$  at the maximum of the

synchrotron spectrum can be estimated as

$$n_{\text{synch}}(\epsilon_{\text{SA}}) = \frac{L_{\text{synch}}}{4\pi R_{\text{synch}}^2 \epsilon_{\text{SA}} c} \quad (25)$$

$$\simeq 10^{17} \left[ \frac{L_{\text{synch}}}{10^{40} \text{ erg/s}} \right] \left[ \frac{R_{\text{synch}}}{10^{12} \text{ cm}} \right]^{-2} \left[ \frac{\epsilon_{\text{SA}}}{0.2 \text{ eV}} \right]^{-1} \text{ cm}^{-3}$$

Using Eq. (24) one finds that because of the sharp cut-off in the synchrotron spectrum above the energy  $\epsilon_{\text{SA}} \sim 0.2 \text{ eV}$ ,  $\gamma$ -rays with energy  $E_\gamma \sim 1 \text{ TeV}$  escape through the synchrotron background,  $\tau_{\gamma\gamma}(E_\gamma = 1 \text{ TeV}) \sim 1$ , if  $R_{\text{synch}} \sim 10^{12} \text{ cm}$  and  $L_{\text{synch}} \lesssim 10^{40} \text{ erg/s}$ . On the other hand, our crude estimates indicate that the spectrum of the escaping  $\gamma$ -rays should be sharply cut-off at the energy  $E_\gamma \simeq 5 [\epsilon_{\text{SA}}/0.2 \text{ eV}]^{-1} \text{ TeV}$ , since  $\tau_{\gamma\gamma}$  rapidly grows to  $\tau_{\gamma\gamma} \gg 1$  at this energy. One should note, however, that the details of the behaviour of the spectrum close to the cut-off strongly depend on the details of the spatial distribution of the synchrotron emission. Since the threshold of the pair production,  $s = 1$  (see Eq. (23)), depends on the angle  $\theta$  between the  $\gamma$ -ray and synchrotron photon velocities, the anisotropy of the synchrotron emission can result in a shift of the cut-off in the  $\gamma$ -ray spectrum toward higher energies.

VHE  $\gamma$ -rays produced outside of the synchrotron emission region, or those which escape from it, pass through the IC background with the photon density:

$$n_{\text{IC}} = \frac{L_{\text{IC}}}{4\pi R_{\text{IC}}^2 \epsilon c} \quad (26)$$

$$\simeq 1.7 \times 10^{11} \left[ \frac{L_{\text{IC}}}{10^{39} \text{ erg/s}} \right] \left[ \frac{R_{\text{IC}}}{10^{14} \text{ cm}} \right]^{-2} \left[ \frac{\epsilon}{1 \text{ eV}} \right]^{-1} \text{ cm}^{-3}$$

The optical depth of this background for the TeV  $\gamma$ -rays can be estimated as

$$\tau_{\gamma\gamma}^{\text{IC}}(E_\gamma) = \sigma_{\gamma\gamma} n_{\text{IC}} R_{\text{IC}} \quad (27)$$

$$\simeq 2.2 \left[ \frac{L_{\text{IC}}}{10^{39} \text{ erg/s}} \right] \left[ \frac{R_{\text{IC}}}{10^{14} \text{ cm}} \right]^{-1} \left[ \frac{E_\gamma}{1 \text{ TeV}} \right]$$

Thus, the inner part of the accretion flow is transparent for the TeV  $\gamma$ -rays if

$$L_{\text{IC}} \lesssim 0.5 \times 10^{39} \left[ \frac{R_{\text{IC}}}{10^{14} \text{ cm}} \right] \left[ \frac{E_\gamma}{1 \text{ TeV}} \right]^{-1} \text{ erg/s}. \quad (28)$$

Finally, the background of the bremsstrahlung radiation does not affect propagation of the high-energy  $\gamma$ -rays. This is due to two reasons: the low density of the corresponding photons and their relatively weak interaction with the VHE  $\gamma$ -rays because of the  $1/s$  suppression of the photon-photon cross-section.

Thus, in the case when the luminosity of the accretion flow is as low as  $L_{\text{acc}} \lesssim 10^{40} \text{ erg/s}$ , the VHE  $\gamma$ -ray emission can originate directly from the vicinity of the black hole. It can be e.g. the direct synchrotron/curvature emission which accompanies the acceleration process. This possibility is illustrated schematically in Fig. 1 (upper panel). Otherwise, if the synchrotron luminosity of RIAF is significantly above  $10^{40} \text{ erg/s}$  and/or the IC luminosity exceeds the limit (28), the VHE  $\gamma$ -ray emission must be produced outside the corresponding radiation regions. This is possible if the primary accelerated particles are protons.

### 2.3.2 Protons

Protons with energies above the threshold

$$E_{\text{th}} = \frac{m_\pi(m_\pi + 2m_P)}{4\epsilon} \sim 8 \times 10^{16} \left[ \frac{\epsilon}{1 \text{ eV}} \right]^{-1} \text{ eV} \quad (29)$$

lose energy in the interactions with the infrared photons of energy  $\epsilon$  via pion production. Near the threshold, the cross-section is dominated by the single pion production resonance  $\sigma_{p\gamma} \sim 6 \times 10^{-28} \text{ cm}^2$ ; in this regime proton gives only 20% of its energy to the pion. At higher proton energies the photo-pion production cross-section decreases down to  $\sigma_{p\gamma} \sim 10^{-28} \text{ cm}^2$ , while the proton energy loss in every interaction increases up to 50%. Thus in both cases protons lose most of their energy at similar distance.

For high synchrotron background,  $L_{\text{synch}} \sim 10^{42} \text{ erg/s}$ , protons with energies  $E_p > 10^{18} \text{ eV}$  cannot escape from the acceleration region,

$$\tau_{p\gamma}^{\text{synch}}(E_p > 10^{18} \text{ eV}) = \sigma_{p\gamma} n_{\text{synch}} R_{\text{synch}} \quad (30)$$

$$\simeq 10^3 \left[ \frac{L_{\text{synch}}}{10^{42} \text{ erg/s}} \right] \left[ \frac{R_{\text{synch}}}{10^{12} \text{ cm}} \right]^{-1} \left[ \frac{\epsilon}{0.2 \text{ eV}} \right]^{-1}.$$

On the other hand, protons with energy  $E_p < 10^{18} \text{ eV}$  interact only with exponential tail of the synchrotron emission and escape from this region.

During the propagation through the inverse Compton emission region at the distance scales  $R \sim 100 R_g$ , protons interact with the inverse Compton photon background, so that the optical depth is

$$\tau_{p\gamma}^{\text{IC}} = \sigma_{p\gamma} n_{\text{IC}} R_{\text{IC}} \quad (31)$$

$$\simeq 0.2 \left[ \frac{L_{\text{IC}}}{10^{41} \text{ erg/s}} \right] \left[ \frac{R_{\text{IC}}}{10^{14} \text{ cm}} \right]^{-1} \left[ \frac{\epsilon}{1 \text{ eV}} \right]^{-1}$$

The power of the absorbed proton flux is converted into the products of pion decays: neutrinos,  $\gamma$ -rays and electrons of the energies  $\sim 0.1 E_p$ . Obviously, the neutrinos freely escape from the production region.

Naively, from the above discussion of propagation of  $\gamma$ -rays, one would expect that  $\gamma$ -rays are not able to escape from such a dense IC background. However, this is incorrect. The point is that the energies of the  $\gamma$ -rays produced in the neutral pion decays are much above the energy corresponding to the maximum of the pair production rate on the IC background. For example, for the  $10^{17} \text{ eV}$   $\gamma$ -rays the cross-section of the pair production on the IC background is  $s/\ln s \sim 10^4$  times smaller than the peak value, so that it is of the order of  $p\gamma$  interaction cross-section. Thus, the mean free path of the secondary  $\gamma$ -rays is comparable to the mean free path of the primary protons and is of order of the size of the IC radiation region. These  $\gamma$ -rays can give rise to electromagnetic cascades redistributing energy into TeV  $\gamma$ -rays. The drawback of this mechanism of TeV emission is its low efficiency (Neronov & Semikoz 2003) due to the fact that the TeV  $\gamma$ -rays which are observed at infinity can be produced only in the surface layer of the IC radiation region, where the optical depth for the TeV radiation drops to the values of order one. On the other hand, this mechanism should result in strong multi-GeV emission which can escape through the whole inverse Compton radiation region without significant absorption. This implies that if this mechanism is indeed responsible for the TeV emission in (some of) the

TeV blazars, it should lead to a strong signal in the multi-GeV band accessible for the Fermi (GLAST) satellite<sup>2</sup>.

Apart from the interactions with soft radiation background, protons can also interact with the matter in the jet. The optical depth of protons with respect to this process is estimated as

$$\tau_{pp} = \sigma_{pp} n_p(R) R, \quad (32)$$

where  $n_p(R)$  is the matter density in the jet at the distance  $R$ . Taking the  $pp$  interaction cross section at energies  $E_p \sim 10^{18}$  eV to be equal to  $\sigma_{pp} \simeq 10^{-25}$  cm<sup>2</sup> we obtain

$$\tau_{pp} \simeq 0.1 \left[ \frac{n_p(R)}{10^8 \text{ cm}} \right] \left[ \frac{R}{10^{16} \text{ cm}} \right]. \quad (33)$$

Particle multiplicity in  $pp$  collisions at  $E_p \sim 10^{18}$  eV is about  $N \sim 100-200$  (see e.g. (Heiselberg 2001) for a review). Thus every collision of a  $10^{18}$  eV proton with a background proton produces  $\sim 100$  photons with  $E_\gamma = 5 \times 10^{15}$  eV from  $\pi^0$ ,  $\sim 100$  neutrinos with the same energy from  $\pi^\pm$  decays and  $\sim 100$  electrons and positrons. All neutrinos escape from the interaction region, while electrons, positrons and photons give rise to an electromagnetic cascade. As we discuss in the next section, this provides a link with the standard picture of VHE emission by relativistic blobs in the jet. The limitation of this mechanism is that it requires rather large densities of matter in the jet, see Eq. (33).

To summarize, the qualitative analysis of this subsection shows that production of VHE  $\gamma$ -rays can, in principle, be possible within the compact source model with proton acceleration, see Fig. 1, lower panel. Still, the details of the mechanism of conversion of the proton flux power into the power of TeV  $\gamma$ -ray emission are yet to be worked out.

#### 2.4 Particle cascade in the accretion flow: a link to the "relativistic blob in the jet" picture

The  $\gamma\gamma$ ,  $p\gamma$  and  $pp$  interactions taking place during the propagation of the high-energy particles through the RIAF environment give rise to electromagnetic cascades, which redistribute the power initially contained in the highest energy particles to the lower energy bands. This is expected to result in the broad-band (radio-to- $\gamma$ -ray) electromagnetic emission from the cascade.

To large extent, this emission can be described by the conventional synchrotron – self Compton and/or synchrotron – external Compton models based on the picture of relativistically moving blobs of plasma in the jet. Indeed, as already mentioned, the primary flow of high-energy particles, accelerated by the compact source, is expected to be highly anisotropic, with the direction set by the magnetic field in the acceleration region. The cascades produce a stream of relativistic particles with velocities scattered within some angle  $\zeta$  around the direction of the primary flow. From the kinematical point of view such a stream is nothing else than a blob of plasma moving with the bulk Lorentz factor

$$\Gamma \simeq \frac{1}{\zeta}. \quad (34)$$

<sup>2</sup> The official website of the Fermi collaboration is <http://fermi.gsfc.nasa.gov/>

The angle  $\zeta$  is determined by the dynamics of the cascade. An important role in this dynamics is played by the value and configuration of the magnetic field. At the late stages of the cascade development, when the density of the particles in the cascade is large, the problem should be solved self-consistently taking into account the back-reaction of the plasma in the cascade on the magnetic field. This observation makes the link between the cascade and the blob pictures not only kinematical but also dynamical: in the standard approach the magnetic field is also determined self-consistently by the dynamics of the blob itself.

Existence of this link enables to use in the analysis of TeV  $\gamma$ -ray flares within the framework of the compact source models many results from the standard approach. In particular, the transparency of the blob for the TeV radiation in the July 2006 large flare of PKS 2155-304 implies the constraint (Begelman et al. 2008)  $\Gamma \gtrsim 50$  and hence,  $\zeta \lesssim 1.1^\circ$ .

On the other hand, there are several important differences between the cascade and a generic relativistic blob model which potentially enable to distinguish the two models observationally. First, in the cascade setup, the relativistic blobs are formed in a compact region close to the black hole. In this way this setup naturally incorporates the observed fast variability and is not in a direct conflict with the low bulk Lorenz factors observed at the parsec-scale distances. Indeed, the bulk motion of the secondary particles in the cascade can decelerate at parsec-scale distances either because of development of intrinsic instabilities or because of interaction with the interstellar medium. To study this possibility, a dynamical numerical calculation of the propagation of the high-energy particle cascade through the accretion flow and through the interstellar medium is needed. Second, the cascade transfers power from the higher-energy particles to the lower-energy ones: in this sense it is a "top-down" scenario of formation of the spectrum of emitting electrons. It would be interesting to understand if the latter property can explain the existence of the low-energy cut-offs in the spectra of electrons in the synchrotron – inverse Compton scenarios (Krawczynski 2007). Finally, as already mentioned, in the compact source model, the emission from the blob may be superimposed onto the  $\gamma$ -ray component originating directly in the acceleration region near the black hole.

### 3 TIMING OF THE SUPERMASSIVE BLACK HOLE IN PKS 2155-304 WITH TEV $\gamma$ -RAYS

Within the compact source model the spectral and variability properties of the VHE signal can be interpreted in a qualitatively different way (as compared to the model of VHE emission from the parsec-scale distances). They can be used to "probe" the physical environment in the central engine: the matter density, the radiative efficiency of the accretion flow, the magnetic field (cf. Rieger & Aharonian (2008b)). Moreover, in this case the VHE observations provide a completely new tool for the study of the black hole physics. Namely, the  $\gamma$ -ray timing data can be used to derive constraints on the parameters of the black hole itself. Below we explore such a possibility on a particular example of the July 2006 large flare of PKS 2155-304 (redshift  $z = 0.116$ ) reported by (Aharonian et al. 2007).

### 3.1 The relevant time scales

Timing properties of emission produced in the vicinity of black hole horizon can be characterized by several fundamental time scales. First, the minimal possible variability time scale is determined by the requirement of causal connection of the emission region and is given by the light crossing time of the black hole horizon,

$$\begin{aligned} t_{lc} &= 2 \left( R_g + \sqrt{R_g^2 - a^2} \right) / c & (35) \\ &\simeq \begin{cases} 10^2 [M_{\text{BH}}/10^7 M_{\odot}] \text{ s}, & a = R_g \\ 2 \times 10^2 [M_{\text{BH}}/10^7 M_{\odot}] \text{ s}, & a = 0 \end{cases} \end{aligned}$$

where  $R_g$  is defined in Eq. (2); the parameter  $a$  is related to the angular momentum  $J_{\text{BH}}$  of the black hole as  $a = J_{\text{BH}}/M_{\text{BH}}c^2$  and lies in the range  $0 \leq a \leq R_g$ .

If the  $\gamma$ -ray emission is produced close to the black hole, variability at the characteristic time scale of rotation around the black hole is expected on general grounds, unless the entire system (the accretion flow with an embedded particle acceleration region) is perfectly axially symmetric. The intensity of the modulation of the signal can depend on various parameters, such as the inclination angle of the observer with respect to the BH rotation axis, distance of the emission region from the horizon, etc. A perfect axial symmetry, which would wash out the modulation of the signal with the period of rotation around the black hole, can be expected in a stationary, quiet state of the source. On the contrary, a bright flare is, most probably, related to rapid change of the system parameters (for example, inspiralling of a denser clump of matter into the black hole) which should lead to a significant disturbance of the axially symmetry.

Close to the horizon of a spinning black hole, the accreting matter rotates around the black hole with the period (Bardeen et al. 1972)

$$P(r) = 2\pi \frac{r^{3/2} \pm aR_g^{1/2}}{cR_g^{1/2}}, \quad (36)$$

where  $r$  is the radius of the orbit. The  $+$  ( $-$ ) sign corresponds to the prograde (retrograde) orbit. It is known that stable circular orbits exist only down to certain distance  $r_{\text{ms}}$  from the BH. The period of rotation along the last prograde stable orbit at the distance  $r_{\text{ms}}$  is

$$P(r_{\text{ms}}) = \begin{cases} 4\pi R_g/c \simeq 630 \left[ \frac{M_{\text{BH}}}{10^7 M_{\odot}} \right] \text{ s}, & a = R_g \\ 12\sqrt{6}\pi R_g/c \simeq 4600 \left[ \frac{M_{\text{BH}}}{10^7 M_{\odot}} \right] \text{ s}, & a = 0 \end{cases} \quad (37)$$

The disturbance of the axial symmetry of the accretion flow is expected to result in the modulation of physical conditions in the AGN central engine with a period given by Eq. (37). Since the properties of the  $\gamma$ -ray emission from the central engine (from the base of the jet) are determined by the physical conditions in the central engine, the modulation of these conditions should result in the modulation of the  $\gamma$ -ray signal with the same period.

### 3.2 Fitting the lightcurve of PKS 2155-304

The VHE  $\gamma$ -ray lightcurve of the flare of PKS 2155-304, reported in (Aharonian et al. 2007), consists of several pronounced sub-flares (see Fig. 2). At least three characteristic time scales can be found in a straightforward way from the

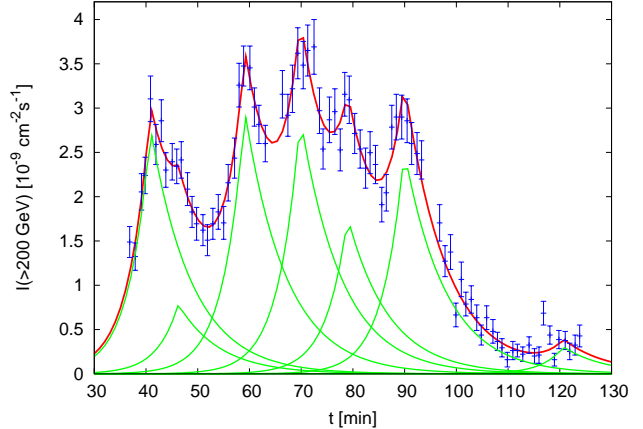


**Figure 2.** The lightcurve of PKS 2155-304 fitted with a sequence of sub-flares with identical profiles, but with different normalizations (see Table 1).

analysis of the lightcurve: the rise and decay times of the individual sub-flares,  $t_{\text{rise}}$ ,  $t_{\text{decay}}$ , and the period of recurrence of the sub-flares,  $T$ . In order to estimate the average values of these parameters we have fitted the VHE lightcurve assuming that the time profiles of the individual sub-flares are characterized by the same rise and decay times, and differ only in the arrival times and the amplitudes<sup>3</sup>. The approximation of identical  $t_{\text{rise}}$ ,  $t_{\text{decay}}$  appears naturally in the context of the compact source models where these parameters are determined by the intrinsic time scales of the central engine, such as e.g. the light crossing time of the black hole and the cascade development time. On the other hand, it is clearly a strong idealization: the complicated dynamics of the particle acceleration and the cascade development is expected to introduce a scatter in the characteristics of the individual sub-flares. Still, we stick to this approximation as a natural first step.

The individual sub-flares are modeled with the profile

$$I_k(t) = \begin{cases} N_k \exp[(t - t_{\text{max},k})/t_{\text{rise}}], & t < t_{\text{max},k} \\ N_k \exp[-(t - t_{\text{max},k})/t_{\text{decay}}], & t > t_{\text{max},k} \end{cases} \quad (38)$$

where the time  $t_{\text{max},k}$  corresponds to the maximum intensity and  $N_k$  is the amplitude of the  $k$ -th sub-flare. Note that we define  $t_{\text{rise}}$  ( $t_{\text{decay}}$ ) as the time in which the signal increases (decreases) by a factor  $e$ . We fit the lightcurve with the sum of several sub-flares (38) and a constant signal. The result of the fit of the overall lightcurve with such a model is shown in Fig. 2. The rise and decay times inferred from the fit are

$$t_{\text{rise}} = (2.5 \pm 0.2) \times 10^2 \text{ s}, \quad (39)$$

$$t_{\text{decay}} = (4.9 \pm 0.5) \times 10^2 \text{ s}, \quad (40)$$

The arrival times  $t_{\text{max},k}$  and normalizations  $N_k$  of the sub-flares are summarized in the Table 1.

Initially, we fitted the lightcurves with a set of five sub-flares which correspond to the five pronounced peaks clearly visible in the data. The quality of this fit was rather low

<sup>3</sup> This model is different from the model considered by (Aharonian et al. 2007) where the rise and decay times were allowed to vary among individual sub-flares.

$k$	$t_{\max,k}$ [min]	$N_k [10^{-9} \text{ cm}^{-2} \text{s}^{-1}]$
1	$40.9 \pm 0.3$	$2.8 \pm 0.3$
2	$46.2 \pm 0.8$	$0.78 \pm 0.24$
3	$59.1 \pm 0.2$	$3.0 \pm 0.17$
4	$69.8 \pm 0.3$	$2.9 \pm 0.2$
5	$79.0 \pm 0.4$	$1.8 \pm 0.2$
6	$89.9 \pm 0.3$	$2.5 \pm 0.2$
9	$120.7 \pm 1.0$	$0.30 \pm 0.11$

**Table 1.** List of parameters of the sub-flares.

( $\chi^2 = 106$  for 70 degrees of freedom). We have found that the addition of one more sub-flare (sub-flare number 2 in Table 1) significantly improves the quality of the fit ( $\chi^2 = 86.3/68$  d.o.f.; the F-test gives a chance probability of the fit improvement at the level of 0.1%). Finally, we have found that the fit can be further improved by addition of one more sub-flare near the end of the overall lightcurve, the last sub-flare in the Table 1. The quality of the fit with seven sub-flares is  $\chi^2 = 75.8/66$  d.o.f. According to the F-test the probability that the latter fit improvement is achieved by chance is 1.4 %.

The arrival times of the six bright sub-flares follow an approximate linear law

$$t_{\max,k} \simeq t_0 + k \cdot T, \quad (41)$$

see Fig. 3. This is reminiscent of quasi-periodic oscillations observed in the X-ray band in the X-ray binaries (van der Klis 2000) and in the infrared band in the Galactic Center (Genzel et al. 2003). The last weak sub-flare also falls on the linear dependence (41) if assigned the number  $k = 9$ . However, we do not use this sub-flare in the following analysis because its presence is not strongly required by the lightcurve fit.

Fitting the set of arrival times  $t_{\max,k}$  of the six bright sub-flares (numbered by 1–6 in the Table 1) with the linear law (41) one finds the recurrence period of the sub-flares,

$$T = (5.93 \pm 0.15) \times 10^2 \text{ s}. \quad (42)$$

This recurrence period coincides with the characteristic variability scale  $\sim 600$  s mentioned by Aharonian et al. (2007).

We have tested if the apparent quasi-periodicity of the signal can appear in the data by chance. To do this we have fixed the arrival times of the first and last of the bright sub-flares (sub-flares 1 and 6 in the Table 1). Then we have allowed the arrival times of the 4 intermediate sub-flares to be distributed randomly between  $t_{\max,1}$  and  $t_{\max,6}$ . The arrival times  $t_{\max,k}$ ,  $k = 1, \dots, 6$  are assigned the errors from the Table 1. We have calculated the probability that fitting the arrival times of the six first sub-flares by the function (41) would result in a  $\chi^2 \leq \chi_0^2$ , where  $\chi_0^2 = 41$  is the  $\chi^2$  of the fit of the real data<sup>4</sup>. This probability turns out to be  $1.3 \cdot 10^{-3}$ . We also tried another error assignment. Namely, all the arrival times were assigned the error  $\delta t = 1.5$  min, which corresponds to the intrinsic scatter of the arrival times

<sup>4</sup> Note that  $\chi_0^2$  is large. This means that the oversimplified model of strictly identical sub-flares with strictly periodic arrival times is actually excluded by the data. This is not surprising: as already mentioned, on physical grounds one expects deviations from this idealization.

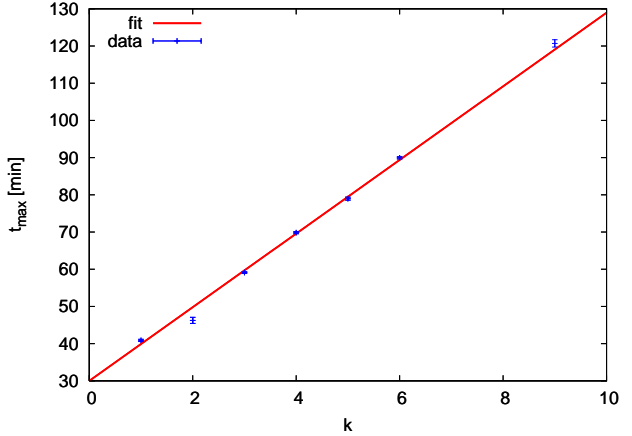


**Figure 3.** The arrival times of the sub-flares of the PKS2155-304 lightcurve as a function of the sub-flare number. The data are fitted by the straight line  $t_{\max,k} = t_0 + k \cdot T$ .

of the real sub-flares around the linear law (41). In this case the best linear fit corresponds to  $\chi_1^2 = 5.43$  for 4 degrees of freedom. The chance probability to obtain  $\chi^2 \leq 5.43$  in the simulated data sets with random arrival times of the intermediate sub-flares turns out to be  $6 \cdot 10^{-3}$  in this case. We have checked that our conclusions do not depend on the particular choice (38) of the sub-flare profile by considering other possible choices of  $I_k(t)$ .

### 3.3 Constraints on the black hole parameters

The rise and decay times (39), (40) as well as the recurrence time (42) are determined by the physics of the  $\gamma$ -ray emission. Within the compact source scenario described in Sec. 2, the minimal possible rise time is given by the light crossing time of the black hole, Eq. (35). Requiring

$$t_{\text{rise}} \geq (1+z)t_{\text{lc}} \quad (43)$$

one finds a range of parameters  $M_{\text{BH}}, a$  excluded by the observations. This range corresponds to the dark shaded region in Fig. 4.

This should be compared with the constraints obtained by other methods. In the literature there are two estimates of the mass of the central black hole in PKS 2155-304.

The first one (Aharonian et al. 2007) is obtained from the relation between the masses of central black holes and luminosities of host galaxy bulges (Bettoni et al. 2003); it gives  $M_{\text{BH}} \sim 10^9 M_{\odot}$ . As it was already noted in (Aharonian et al. 2007), this estimate is in conflict with the constraint  $M_{\text{BH}} \leq 2 \times 10^7 M_{\odot}$  derived from the  $\gamma$ -ray variability properties. We point out, however, that there are several uncertainties in the estimate based on the  $M_{\text{BH}} - L_{\text{bulge}}$  relation. It is obtained by extrapolating the empirical relation observed in a local sample of normal galaxies to the case of TeV blazars. The reliability of this extrapolation was never investigated. Besides, the relation itself has a large intrinsic scatter (order-of-magnitude deviations are present). Finally, there is no consensus in the literature about the luminosity of the host galaxy in PKS 2155-304 (see (Aharonian et al. 2007) and references therein).

The second estimate (Zhang et al. 2005) is based on

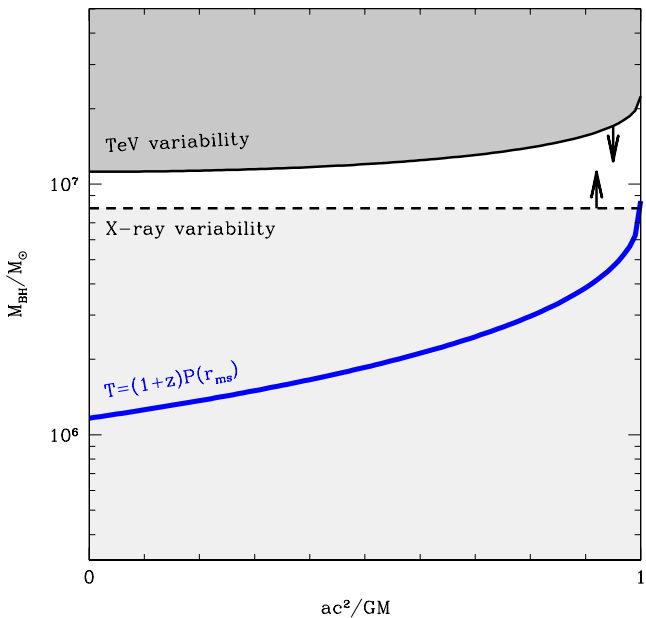


**Figure 4.** The parameters of the supermassive black hole in PKS 2155-304 inferred from the VHE  $\gamma$ -ray lightcurve. The shaded region shows the range of  $M_{\text{BH}}$ ,  $a$  excluded by the requirement (43). Thick blue curve shows the relation between  $M_{\text{BH}}$  and  $a$  obtained by identifying the period of the sub-flare recurrence with the rotation period over the last stable orbit. The horizontal line shows the lower bound on the black hole mass implied by the X-ray variability analysis of (Zhang et al. 2005). For  $a > 0$  this bound should be taken with caution as its dependence on  $a$  has not been explored.

the study of X-ray variability properties of PKS 2155-304: it uses the method of (Nikolajuk et al. 2004) to relate the mass of black hole to the excess variability  $\sigma_{\text{nxs}}^2$  at a certain frequency scale. This method yields the bound  $M_{\text{BH}} \geq 8.1 \times 10^6 M_{\odot}$ , shown by a dashed horizontal line in Fig. 4. The latter estimate is compatible with the constraint derived from the TeV variability of the source. One should note, however, that the estimate of the black hole mass based on the X-ray variability properties suffers from the same uncertainty as the estimate based on the  $M_{\text{BH}} - L_{\text{bulge}}$  relation: it is originally derived for a sample of nearby non-blazar AGNs. Its applicability to the sample of the TeV blazars was never tested.

The tight constraint on the black hole mass, derived from the TeV variability time scale, provides a possibility of strong observational test of the compact source model. Indeed, a precise determination of the black hole mass by another method would be able to falsify or confirm the compact source model.

The indication of the quasi-periodicity of the sub-flare arrival times suggests to associate the period  $T$  of the sub-flare recurrence with the (minimal possible) period of rotation around the black hole,

$$T = (1 + z)P(r_{\text{ms}}). \quad (44)$$

This gives a relation between  $a$  and  $M_{\text{BH}}$  shown by the thick blue curve in Fig. 4. If combined with the constraint on the black hole mass derived from the X-ray variability analysis (Zhang et al. 2005), this relation implies that the black

hole is rotating almost at the maximal rate,  $a \approx R_g$ . However, we remind that the X-ray constraint on the black hole mass should be taken with caution. In particular, to the best of our knowledge, the dependence of this phenomenological constraint on the black hole spin  $a$  has not been explored.

#### 4 CONCLUSIONS

In this paper we have proposed that the recently observed fast variability of the VHE emission from blazars can be naturally accommodated within the framework of "compact source" model. In this model particles responsible for the observed VHE emission are accelerated close to the central supermassive black hole, rather than at large distances downstream the AGN jet. We have analyzed the problem of escape of the VHE  $\gamma$ -rays from the vicinity of the central engine and demonstrated that the region around the central engine is transparent for TeV  $\gamma$ -rays if the accretion flow in the TeV blazars is radiatively inefficient. If the luminosity of the accretion flow is as low as  $L_{\text{acc}} \lesssim 10^{40} \text{ erg/s}$ , the TeV  $\gamma$ -ray emission can come directly from the immediate neighborhood of the central black hole. Alternatively, for brighter accretion flows, the TeV  $\gamma$ -rays may be produced at some distance from the black hole in a proton-initiated electromagnetic cascade developing in the accretion flow.

The possibility that the properties of the VHE  $\gamma$ -ray emission are directly linked to the properties of the central engine of the AGN, if confirmed by future observations, provides a new tool to study the physical conditions in the direct vicinity of the supermassive black hole. In particular, the VHE signal can be used to constrain the parameters of the accretion flow and of the black hole itself, such as its mass and spin.

We demonstrated this possibility on the example of the bright TeV flare of the blazar PKS 2155-304. Within the proposed scenario, the characteristic time scales, found in the timing analysis of this flare, are directly related to the parameters of the supermassive black hole. The minimal variability time scale of the signal is identified with the black hole light-crossing time. This sets the bound on the black hole mass and its rotation moment shown in Fig. 4. We also observed that the signal exhibits quasi-periodic oscillations. Identifying the recurrence time of these oscillations with the period of rotation around the black hole we obtained a relation between the black hole mass and its rotation moment.

A detailed modeling based of the framework proposed in this paper should involve calculation of particle acceleration and propagation in the vicinity of the black hole through the environment created by the accretion flow. This can be done assuming particular (numerical) models of RIAF and particle acceleration. We leave this for future work.

#### Acknowledgments

We thank F. Bezrukov, A. Boyarsky, G. Dvali, D. Horns, K. Postnov, V. Rubakov, O. Ruchayskiy, G. Sigl, P. Tinyakov and I. Tkachev for useful discussions and comments. The work of S.S. was partially supported by the EU 6th Framework Marie Curie Research and Training network "UniverseNet" (MRTN-CT-2006-035863). D.S. thanks The

oretical Department of CERN for hospitality during initial stages of this work.

## APPENDIX A: SYNCHROTRON SELF-ABSORPTION IN THE ACCRETION FLOW

The function  $I(x)$  entering into the expression (14) for the synchrotron self-absorption coefficient has the form (Pacholczyk 1970),

$$I(x) = \frac{1}{x} \int_0^\infty z^2 e^{-z} F(x/z^2) dz, \quad (A1)$$

where  $F(x) = x \int_x^\infty K_{5/3}(z) dz$ . It is straightforward to obtain the asymptotics of  $I(x)$ ,

$$I(x) \sim \sqrt{2/3\pi} \exp(-3(x/4)^{1/3}), \quad x \gg 1. \quad (A2)$$

The synchrotron photons are self-absorbed below a certain energy  $\epsilon_{SA}$ . The latter is estimated from the condition that the optical depth for the synchrotron emission with energy  $\epsilon_{SA}$  is equal to unity,

$$\alpha_{SA}(\epsilon_{SA}) R_{synch} = 1, \quad (A3)$$

where  $R_{synch}$  is the size of the synchrotron emission region. Taking  $R_{synch} \approx R_g$  one obtains the following equation for the variable<sup>5</sup>  $x_{SA}$  corresponding to the self-absorption energy  $\epsilon_{SA}$ ,

$$1.89x_{SA}^{1/3} + \ln x_{SA} = 17.37 \\ + \ln \left\{ \left[ \frac{n}{10^{10} \text{ cm}^{-3}} \right] \left[ \frac{M_{BH}}{10^7 M_\odot} \right] \left[ \frac{B}{10^4 \text{ G}} \right]^{-1} \left[ \frac{T_e}{1 \text{ MeV}} \right]^{-5} \right\}. \quad (A4)$$

When the logarithm in the second line vanishes, the solution to this equation is

$$x_{SA} = 247. \quad (A5)$$

This corresponds to the value (16) of the self-absorption energy. Note that the r.h.s. of the equation (A4) logarithmically depends on the parameters of the accretion flow implying that the variable  $x_{SA}$  is only mildly sensitive to these parameters. Namely, the value (A5) is multiplied by a factor ranging from 0.6 to 1.5 when the combination of the parameters entering the logarithm in the second line of Eq. (A4) varies from 0.1 to 10.

## REFERENCES

Aharonian, F., et al. 2003, A&A, 403, L1  
 Aharonian, F., & Neronov, A. 2005, Ap.J., 619, 306  
 Aharonian, F., Akhperjanian, A. G., Bazer-Bachi, A. R., & et al. 2006, Science, 314, 1424  
 Aharonian, F., et al. 2007, Ap.J., 664, L71  
 Albert, J., et al. 2007, Ap.J., 669, 862  
 Albert, J., et al. 2008, arXiv:0806.0988.  
 Bardeen, J.M., Press, W.H., Teukolsky, S.A., 1972, Ap.J. 178, 347.

Bednarek, W., & Protheroe, R. J. 1999, MNRAS, 302, 373 [arXiv:astro-ph/9802288]  
 Begelman, M. C., Fabian, A. C., & Rees, M. J. 2008, MNRAS, 384, L19  
 Bettoni, D., Falomo, R., Fasano, G., & Govoni, F. 2003, A&A, 399, 869  
 Blandford R.D., Levinson A., 1995, Ap.J. 441, 79  
 Browne, I. W. A. 1983, MNRAS, 204, 23P  
 Celotti, A., Fabian, A. C., Rees, M. J., 1998, MNRAS, 293, 239  
 Genzel, R., Schödel, R., Ott, T., Eckart, A., Alexander, T., Lacombe, F., Rouan, D., & Aschenbach, B. 2003, Nature, 425, 934  
 Ghisellini, G., & Madau, P. 1996, MNRAS, 280, 67  
 Giroletti, M., Giovannini, G., Taylor, G. B., & Falomo, R. 2004, Ap.J., 613, 752  
 Giroletti, M., Giovannini, G., Taylor, G. B., & Falomo, R. 2006, Ap.J., 646, 801  
 Henri & Saugé, 2006, Ap.J., 640, 185  
 Heiselberg, H. 2001, Physics Reports, 351, 161 [arXiv:nucl-th/0003046]  
 Kardashev, N. S. 1995, MNRAS, 276, 515  
 Krawczynski, H. 2007, Ap.J., 659, 1063  
 Levinson, A. 2000, Physical Review Letters, 85, 912  
 Lesch, H., & Pohl, M. 1992, A&A, 254, 29  
 Lovelace, R. V. E. 1976, Nature, 262, 649  
 Lu, J.-F., Li, S.-L., & Gu, W.-M. 2004, MNRAS, 352, 147  
 Narayan, R. 2002, in *Lighthouses of the Universe: The Most Luminous Celestial Objects and Their Use for Cosmology*, ed. M. Gilfanov, R. Sunyaev, E. Churazov. (Springer-Verlag), 405; arXiv:astro-ph/0201260  
 Narayan, R., & Yi, I. 1994, Ap.J., 428, L13  
 Narayan, R., & Yi, I. 1995, Ap.J., 452, 710  
 Neronov, A., Semikoz, D., Aharonian, F., & Kalshev, O. 2002, Physical Review Letters, 89, 051101 [arXiv:astro-ph/0201410]  
 Neronov, A. Y., & Semikoz, D. V. 2002, Physical Review D, 66, 123003 [arXiv:hep-ph/0208248]  
 Neronov, A., & Semikoz, D. 2003, New Astronomy Review, 47, 693  
 Neronov, A., Tinyakov, P., & Tkachev, I. 2005, Journal of Experimental and Theoretical Physics, 100, 656 [Zh. Eksp. Teor. Fiz. 100, 744] [arXiv:astro-ph/0402132]  
 Neronov, A., & Aharonian, F. A. 2007, Ap.J., 671, 85  
 Neronov, A., Semikoz, D., Tkachev, I. 2008, *Ultra-High Energy Cosmic Ray production in the polar cap regions of black hole magnetospheres*, arXiv:0712.1737 [astro-ph], submitted to JETP  
 Nikolajuk, M., Papadakis, I. E., & Czerny, B. 2004, MNRAS, 350, L26  
 Pacholczyk, A. G., 1970, *Radio Astrophysics*, (W.H. Freeman and company, San Francisco)  
 Piner, B. G., Pant, N., & Edwards, P. G. 2008, Ap.J., 678, 64  
 Rees, M. J., Begelman, M. C., Blandford, R. D., & Phinney, E. S. 1982, Nature, 295, 17  
 Rieger, F. M., & Aharonian, F. A. 2008a, A&A, 479, L5  
 Rieger, F. M., & Aharonian, F. A. 2008b, arXiv:0805.4075  
 Rybicki G. B., Lightman A. P., 2004, *Radiative Processes in Astrophysics*, Wiley-VCH.  
 van der Klis, M. 2000, ARA&A, 38, 717  
 Zhang, Y. H., Treves, A., Celotti, A., Qin, Y. P., & Bai,

<sup>5</sup> See Eq. (15) for the definition of this variable.

